Morphological Snakes

Luis Álvarez[‡] Luis Baumela[†] Pedro Henríquez[‡] Pablo Márquez-Neila[†]

[‡]Dep. Informática y Sistemas
Universidad de las Palmas de Gran Canaria
http://ami.dis.ulpgc.es/

[†]Dep. Inteligencia Artificial
Facultad Informática
Universidad Politécnica de Madrid
http://www.dia.fi.upm.es/ pcr

Abstract

We introduce a morphological approach to curve evolution. The differential operators used in the standard PDE snake models can be approached using morphological operations on a binary level set. By combining the morphological operators associated to the PDE components we achieve a new snakes evolution algorithm. This new solution is based on numerical methods which are very simple, fast and stable. Moreover, since the level set is just a binary piecewise constant function, this approach does not require to estimate a contour distance function. To illustrate the results obtained we present some numerical experiments on real images.

1. Introduction

Snakes and their geometrically sound alternative, geodesic active contours [2], are possibly the most popular curve evolution algorithms. By iteratively solving a partial differential equation (PDE), the curve or snake deforms its shape so as to minimize internal and external energies along its boundary. The internal component keeps the curve smooth, while the external component attaches the curve to image structures, such as edges, lines, etc. This scheme has many desirable properties such as its parameterization-free nature, intuitive formulation and ability to adapt to shapes of unknown topology. This behavior makes curve evolution one of the most widely used algorithms for image segmentation and object tracking.

Our work is related to many previous results whose aim is to achieve efficient and robust curve evolution algorithms, e.g. [1, 5, 9, 10]. The level set approach has been successfully used to perform curve evolution. The main steps of this method are : (i) the contour is included in a level set computing the contour signed distance function, (ii) the PDE model is solved in a contour narrow band and (iii) Reinitialization of the contour and the distance function is required in order to keep the stability of the algorithm. Goldenberg and colleagues use the narrow-band approach with an unconditionally stable numerical scheme (Additive Operator Splitting) and multi-resolution for a stable active contour evolution [5]. Paragios [9] also uses the Additive Operator Splitting schema with a boundary force, the gradient vector field, to guide the curve evolution. Shi and Karl [10] adopt a completely different approach. Instead of solving the PDE, the evolution of the curve is realized by simple operations such as switching elements between two linked lists of pixels representing the contour. Regularization is achieved by Gaussian filtering.

The main contribution of this paper is a new morphological approach to the solution of the PDE associated to snake model evolution. That is, we approach the solution of the PDE using just $\inf$-$\sup$ operators. This is based on the observation that the differential operators involved in the PDE snakes evolution model can be approached using morphological operators and the solution of the PDE can be approximated as a composition of such morphological operators.

The main advantage of this solution is that the level set is much simpler to define (we can take just 0 outside the contours an 1 inside). Also, the contour evolution algorithm is much faster that the usual level set method because we only use the $\inf$-$\sup$ operator. We do not need to perform a finite difference numerical implementation of the differential operator, which are much more sophisticated and time consuming than the $\inf$-$\sup$ operators. Moreover, no reinitialization of the level set and contour is needed. So these nice properties of our approach enables us to devise a very fast and stable curve evolution algorithm. For a general the-

oretical introduction to the relation between morphological operator and geometric PDE solutions see [6].

2. Active Contours and level sets

Let $\mathcal{C} : [0,1] \to \mathbb{R}^2$ be a parametrized 2D curve and $I : \mathbb{R}^2 \to \mathbb{R}$ be an image. The evolution of curve $\mathcal{C}$ over time is due to the effect of a scalar field $\mathcal{F}$ which deform the curve along its inwards normals, *i.e.*, $\mathcal{C}_t = \mathcal{F} \cdot \mathcal{N}$. In the specific case of the geodesic active contours [2], $\mathcal{F} = g(I)\mathcal{K} + g(I)\nu - \nabla g(I) \cdot \mathcal{N}$, where $\mathcal{K}$ is the Euclidean curvature of $\mathcal{C}$, $\nu \in \mathbb{R}$ is the balloon force parameter (see [4]) and $g(I)$ selects which regions of image I attract the curve. Typically, $g(I)$ could be

$$g(I) = \frac{1}{\sqrt{1 + \alpha |\nabla G_\sigma * I|}}, \tag{1}$$

which is low in the edges of the image, or

$$g(I) = |G_\sigma * I| \tag{2}$$

which attains its minima at the center of the image dark lines. The Osher-Sethian [8] level set method represents the curve in an implicit form as the level set of an embedding function. Let $u : \mathbb{R}^+ \times \mathbb{R}^2 \to \mathbb{R}$ be an implicit representation of $\mathcal{C}$ such that $\mathcal{C}(t) = \{(x,y); u(t,(x,y)) = 0\}$. It is easy to see that, if the curve evolution has the form $\mathcal{C}_t = \mathcal{F} \cdot \mathcal{N}$, the evolution of any function $u(x,y)$ which embeds the curve as one of its level sets is

$$\frac{\partial u}{\partial t} = \mathcal{F} \cdot |\nabla u|. \tag{3}$$

See [7] or the Appendix C in [2] for a proof. Knowing that the curvature $\mathcal{K}$ can be computed with the information on the function u as $\mathcal{K} = \text{div}\left(\frac{\nabla u}{|\nabla u|}\right)$, we get the well-known curve evolution for the geodesic active contours in a level set framework:

$$\frac{\partial u}{\partial t} = g(I)|\nabla u| \left(\text{div}\left(\frac{\nabla u}{|\nabla u|}\right) + \nu \right) + \nabla g(I) \nabla u. \tag{4}$$

The flow given by this expression has three components, two of them related to the internal energy of the curve and one of them related to the external energy. The internal energy components are the smoothing operator, which tends to smooth the curve at high curvature segments, and the balloon balloon, which *inflates* or *deflates* the curve in areas of little information. The external energy component is responsible for bringing the curve to the interesting regions of the image.

Differential equation (4) can be solved with numerical integration methods such as a finite-difference scheme. However, these techniques are sensitive to the step size, converge slowly and may diverge. In the following section we introduce a morphological approach to curve evolution which is simpler, faster and more stable.

3. Morphological evolution of geodesic active contours

Inspired by the active contour PDE (4), we propose a new morphological evolution method that solves the PDE but avoids the problems of speed and convergence associated to the numerical algorithms. The new evolution will use a combination of binary morphological operators whose infinitesimal behavior is equivalent to the flow expressed by the equation (4). Therefore, the curve is given as the zero level set of a binary piecewise constant function $u : \mathbb{R}^2 \to \{0,1\}$. We take $u(x) = 1$ for every point x inside the curve, and $u(x) = 0$ for every point x outside the curve. The morphological operators will act on u and, hence, they will implicitly evolve the curve.

3.1. Balloon force operator

The erosion and dilation are two well-known morphological operators. The dilation of a function is defined as $(D_h u)(\mathbf{x}) = \sup_{\mathbf{y} \in hB} u(\mathbf{x} - \mathbf{y})$, and the erosion is $(E_h u)(\mathbf{x}) = \inf_{\mathbf{y} \in hB} u(\mathbf{x} - \mathbf{y})$. In both cases, h is the radius of the operator, and B is a disk with radius 1.

Let us study the behavior of these operators in terms of continuous-scale morphology. The function $u_d : \mathbb{R}^+ \times \mathbb{R}^2 \to \mathbb{R}$ defined as $u_d(t,\mathbf{x}) = D_t u_0(\mathbf{x})$ is the solution to the following partial differential equation:

$$\frac{\partial u_d}{\partial t} = |\nabla u_d| \tag{5}$$

for the initial condition $u_d(0,\mathbf{x}) = u_0(\mathbf{x})$ (see [7] for a proof). Therefore, D_h is the infinitesimal generator of the PDE in eq. (5) and we can verify that

$$\lim_{h \to 0^+} \frac{D_h u - u}{h} = |\nabla u|. \tag{6}$$

With a similar reasoning, we can say that the function $u_e : \mathbb{R}^+ \times \mathbb{R}^2 \to \mathbb{R}$ defined as $u_e(t,\mathbf{x}) = E_t u_0(\mathbf{x})$ is the solution to the PDE

$$\frac{\partial u_e}{\partial t} = -|\nabla u_e| \tag{7}$$

for the initial condition $u_e(0,\mathbf{x}) = u_0(\mathbf{x})$. These results allow us to solve a level set evolution PDE like those on equations (5) and (7) using the morphological operators D_h and E_h, respectively.

We will focus on the balloon type operator term of equation (4):

$$\frac{\partial u_{\text{ball}}}{\partial t} = g(I) \cdot \nu \cdot |\nabla u_{\text{ball}}|. \tag{8}$$

The factor $g(I)$ controls the strength of the balloon force in different segments of the curve: when $g(I)$ is high, the corresponding segment is located far from a target region, and the balloon force must be strong; on the other hand,

when $g(I)$ becomes lower, the curve is approaching its objective, and hence the balloon force becomes unnecessary. The effect of the $g(I)$ factor in (8) can be discretized with a single threshold θ: when $g(I)$ is greater than θ, the corresponding point is updated according to the balloon force, and left unchanged otherwise. Depending on the value of ν, the remaining factors ($\nu \cdot |\nabla u_{\text{balloon}}|$) lead to the dilation and the erosion PDEs given above. Given the snake evolution at iteration n, $u^n : \mathbb{R}^2 \to \{0, 1\}$, the balloon force PDE (8) applied over u^n can be solved using the following morphological approach:

$$u^{n+1}(\mathbf{x}_i) = \begin{cases} (D_d u^n)(\mathbf{x}_i) & \text{if } g(I)(\mathbf{x}_i) > \theta \text{ and } \nu > 0 \\ (E_d u^n)(\mathbf{x}_i) & \text{if } g(I)(\mathbf{x}_i) > \theta \text{ and } \nu < 0 \\ u^n(\mathbf{x}_i) & \text{otherwise} \end{cases}, \tag{9}$$

where D_d and E_d are the discrete versions of dilation and erosion.

3.2. Smoothing morphological operator

Let $\mathcal{B}$ the set of all line segments of length 2 centered at the origin of $\mathbb{R}^2$. We define the morphological continuous line operators as

$$(SI_h u)(\mathbf{x}) = \sup_{B \in \mathcal{B}} \inf_{\mathbf{y} \in \mathbf{x} + hB} u(\mathbf{y}), \tag{10}$$

$$(IS_h u)(\mathbf{x}) = \inf_{B \in \mathcal{B}} \sup_{\mathbf{y} \in \mathbf{x} + hB} u(\mathbf{y}). \tag{11}$$

The *mean operator*

$$(F_h u)(\mathbf{x}) = \frac{(SI_h u)(\mathbf{x}) + (IS_h u)(\mathbf{x})}{2} \tag{12}$$

has some interesting properties. The so-called Catté-Dibos-Koepfler scheme [3] relates the operator F_t with the mean curvature motion in the following manner:

$$(F_h u)(\mathbf{x}) = u(\mathbf{x}) + h^2 \frac{1}{4} |\nabla u| \operatorname{div}\left(\frac{\nabla u}{|\nabla u|}\right)(\mathbf{x}) + O(h^3). \tag{13}$$

Rearranging terms and setting a small h, we obtain the infinitesimal generator of the F_h operator:

$$\lim_{h \to 0^+} \frac{(F_{\sqrt{4h}} u)(\mathbf{x}) - u(\mathbf{x})}{h} = |\nabla u| \operatorname{div}\left(\frac{\nabla u}{|\nabla u|}\right)(\mathbf{x}). \tag{14}$$

Subsequently, we can solve the mean curvature motion by means of the F_h operator. Unfortunately, one can easily see that F_h is no longer a morphological operator in the sense that it generates new level set values. We can avoid this problem using operator composition. Given any two operators T_h^1 and T_h^2, we have, for a small h, that

$$T_{h/2}^2 \circ T_{h/2}^1 u \approx \frac{T_h^2 u + T_h^1 u}{2}. \tag{15}$$

See Appendix A for the proof.

Therefore, the non-morphological operator $F_{\sqrt{4h}}$ can be approximated by the morphological operator $SI_{\sqrt{h}} \circ IS_{\sqrt{h}}$. We will iterate this new operator in order to approach the solution of the weighted mean curvature PDE:

$$\frac{\partial u_{smt}}{\partial t} = g(I) \cdot |\nabla u_{smt}| \cdot \operatorname{div}\left(\frac{\nabla u_{smt}}{|\nabla u_{smt}|}\right). \tag{16}$$

As in the previous case, the $g(I)$ factor acts like a weight which controls the strength of the smoothing operation at every point, and we will discretize it again by means of a threshold θ. The morphological evolution of the PDE (16) for a known function u^n is given by

$$u^{n+1}(\mathbf{x}_i) = \begin{cases} (SI_d \circ IS_d u^n)(\mathbf{x}_i) & \text{if } g(I)(\mathbf{x}) > \theta \\ u^n(\mathbf{x}) & \text{otherwise} \end{cases}, \tag{17}$$

where SI_d and IS_d are the discrete versions of the above morphological continuous line operators. Both IS_d and SI_d have their own version of the set $\mathcal{B}$, $\mathcal{P}$, which is a collection of four discretized segments centered at the origin:

$$\mathcal{P} = \left\{ \begin{array}{c} \{(0,0),(1,0),(-1,0)\}, \\ \{(0,0),(0,1),(0,-1)\}, \\ \{(0.0),(1,1),(-1,-1)\}, \\ \{(0,0),(1,-1),(-1,1)\} \end{array} \right\}. \tag{18}$$

3.3. How does the $SI_d \circ IS_d$ operator work?

Here we present an intuitive explanation of the $SI_d \circ IS_d$ smoothing operator. In binary images u, both SI_d and IS_d perform the same operation, but SI_d works only on white (or *active*) pixels and IS_d only on black (or *inactive*) pixels. It is easy to see that SI_d does not affect inactive pixels. Suppose $u(\mathbf{x}_0)$ is an inactive pixel, *i.e.*, $u(\mathbf{x}_0) = 0$. Then, $\inf_{\mathbf{y} \in \mathbf{x}_0 + P} u(\mathbf{y})$ will be 0 for every segment P in $\mathcal{P}$, and therefore $(SI_d u)(\mathbf{x}_0) = 0$. Following a similar reasoning, we can see that IS_d does not affect active pixels.

For every active pixel $\mathbf{x}_1$ in a binary image, the SI_d operator looks for small (3 pixels long) straight lines of active pixels which contain $\mathbf{x}_1$. This search is done in the four possible orientations corresponding to the four segments in $\mathcal{P}$. If no straight line exists, the pixel is made inactive (see Figure 1). Sharp edges (Fig. 1c and 1d) are detected as those pixels which are not part of a straight line and removed. The active pixels in smooth edges (Fig. 1a and 1b) remain unchanged.

For inactive pixels, the IS_d operator carries out a similar procedure (see Figure 2).

The composition $SI_d \circ IS_d$ first removes the sharp inactive pixels with IS_d, and then repeats the procedure for the active ones with SI_d. The result is a global smoothing of u, as can be seen in the Figure 3.

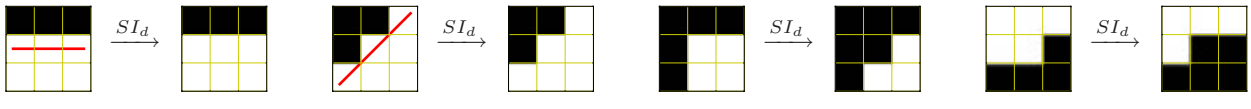

Figure 1. Some examples of the effect of the SI_d operator on individual pixels of binary images. In those cases where a straight line is found (marked in red), the central pixel remains active ((a) and (b)). When the central pixel does not belong to a straight line of active pixels, it is made inactive ((c) and (d)). For exemplification purposes, we assume the pixels on the borders are not affected by the operator.

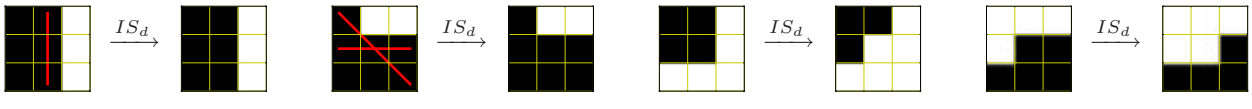

Figure 2. Examples of the IS_d operator.

Note that the examples (d) in the Figures 1 and 2 show opposite cases. Occasionally, the IS_d operator may consider an inactive pixel as *sharp*, and make it active. But then, SI_d also considers *sharp* that pixel and makes it inactive again. The composition $SI_d \circ IS_d$ leaves these pixels unchanged:

$$SI_d \circ IS_d \left(\quad \right) = SI_d \left(\quad \right) = \quad . \qquad (19)$$

3.4. Solving the complete PDE

As we stated above, the active contour equation (4) is made up of three different components: a smoothing force, a balloon force and an attraction force. In previous sections we have seen how two of these components may be solved with morphological operators. The third component, *i.e.*, the attraction force, has an immediate discrete version as we will see shortly.

In the PDE, the combination of the three components is performed through their addition. Our morphological solution will combine them by alternating their discretized approaches: in each iteration, we will apply the morphological ballon (8), the morphological smoothing (16) and the discretized attraction force over the embedding level set function u. Given the snake evolution at iteration n, $u^n : \mathbb{R}^2 \to \{0, 1\}$, we define u^{n+1} from u^n using the following steps:

$$u^{n+\frac{1}{3}}(\mathbf{x}) = \begin{cases} (D_d u^n)(\mathbf{x}_i) & \text{if } |\nu| g(I)(\mathbf{x}_i) > \theta \\ & \quad \text{and } \nu > 0 \\ (E_d u^n)(\mathbf{x}_i) & \text{if } |\nu| g(I)(\mathbf{x}_i) > \theta \\ & \quad \text{and } \nu < 0 \\ u^n(\mathbf{x}_i) & \text{otherwise} \end{cases},$$

$$u^{n+\frac{2}{3}}(\mathbf{x}_i) = \begin{cases} 1 & \text{if } \nabla u^{n+\frac{1}{3}} \nabla g(I)(\mathbf{x}_i) > 0 \\ 0 & \text{if } \nabla u^{n+\frac{1}{3}} \nabla g(I)(\mathbf{x}_i) < 0 \\ u^{n+\frac{1}{3}} & \text{if } \nabla u^{n+\frac{1}{3}} \nabla g(I)(\mathbf{x}_i) = 0 \end{cases},$$

$$u^{n+1}(\mathbf{x}_i) = \begin{cases} (SI_d \circ IS_d u^{n+\frac{2}{3}})(\mathbf{x}_i) & \text{if } g(I)(\mathbf{x}) > \theta \\ u^{n+\frac{2}{3}}(\mathbf{x}) & \text{otherwise} \end{cases},$$

which is the morphological implementation of the active contour PDE. The new ν factor in the first step allows us to set a different threshold level for the balloon operator than for the smoothing operator. Thus we can control the strength of the balloon operator.

4. Results

In order to assess the performance of the morphological snakes method, we have evolved contours in various images. Figure 4 shows several frames of the contour evolution in the *soccer* image. This image was taken in a toy soccer scenario, and it has some challenging features: isolated components (three players and a soccer ball) with elongated elements (player's arms and legs) and some areas with difficult access (pixels enclosed by the third player's arms). As we can see, the morphological evolution deals correctly with these problems: it segments all elements separately, and penetrates well in difficult regions (frame 145 shows the point at which the snake enters in two of these regions). Since the *soccer* image has a low noise level and presents fine details, we picked a small kernel size ($\sigma = 0.14$). As it is a large image and the contour was initialized far from the optimum, it took up to 210 iterations until convergence with a weak eroding balloon force ($\nu = -0.1$).

Figure 5 shows some results with two ultrasound images of breast nodules. This kind of images are characterized by a high noise level and a cluttered look. For that reason,

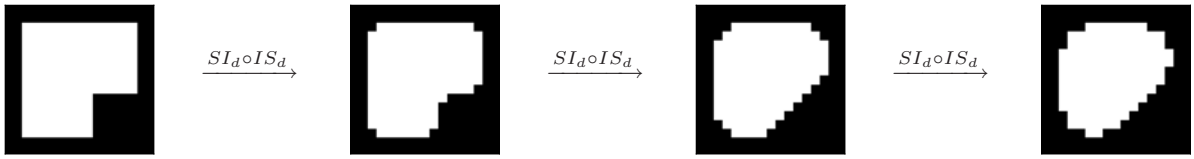

Figure 3. Example of the $SI_d \circ IS_d$ operator iterated until convergence.

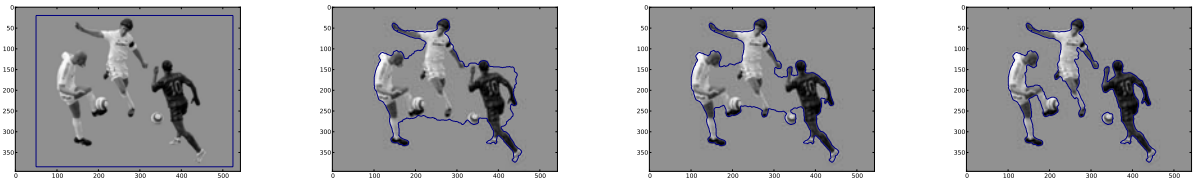

Frame 0 Frame 120 Frame 145 Frame 210

Figure 4. Morphological active contours on the *soccer* image. The image showed here is a cropped 543×396 version of the original 3008×2000 image.

Image	Image size	ν	θ	σ
Soccer	3008×2000	-0.1	0.05	0.14
Medical1	256×256	0.32	0.1	5.48
Medical2	256×256	0.32	0.1	5.48

Table 1. Parameters used in experiments: balloon operator strength ν, threshold θ and convolution kernel size σ (for $g(I)$).

Image	GeoAct. Contours	Morph. Snakes
Soccer	407s	23s
Medical1	8.1s	1.1s
Medical2	8.3s	1.2s

Table 2. Execution times of geodesic active contours and morphological snakes for each image.

we used a big convolution kernel ($\sigma = 5.48$), which helps the snake to avoid, to some extent, the effect of noise. In these images, the evolution takes around 70 iterations until convergence.

The choice of the parameter θ is not trivial. We obtained good results by setting it to be smaller than the 90% of the gray values in $g(I)$. This can be fitted using a histogram of $g(I)$ values. The parameters ν and σ were set based on the image I and on the characteristics of its borders in the same way as in the classical Geodesic Active Contours method. We processed all images using the edge detector of equation (1). Its parameter α was fixed to 1000, but we found that other values do not significantly affect the results. The specific parameters used in each experiment are listed in Table 1.

Finally, we performed quantitative comparisons of running times between Morphological Snakes and a standard method for curve evolution based on solving the PDE. We ran the previous experiments with our Morphological Snakes C++ implementation and the Geodesic Active Contours C++ code of the *Insight segmentation and registration toolkit* [11], which implements a finite-difference method to solve the PDE. Table 2 shows the results of each run. The improvement in performance achieved by our method is roughly one order of magnitude.

5. Conclusions

In this paper we have presented the morphological snakes, a new approach to active contours evolution using a morphological implementation of the underlying PDE. This scheme offers notable advantages over the numerical solutions of the PDE. First, the curve evolution is simpler and faster. Second, the morphological snakes do not suffer from instability problems. Third, since the embedding function does not represent a distance, it requires no re-initialization.

The numerical experiments we have conducted are very promising. We obtain good segmentation results in a variety of images. The performance is approximately one order of magnitude faster than the standard finite-difference method.

The algorithm source code can be downloaded from the Web site `http://www.ipol.im`.

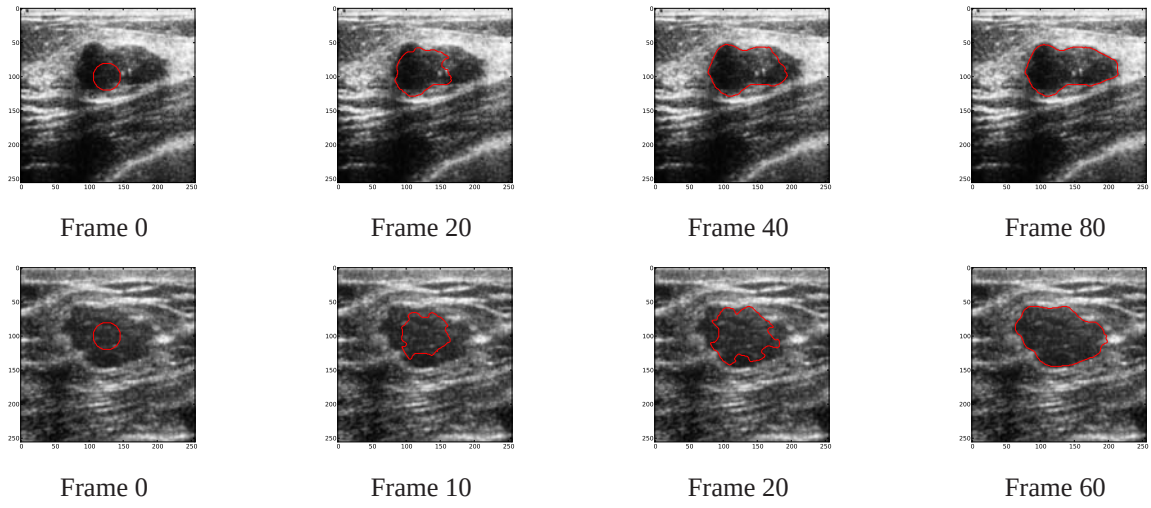

Figure 5. Morphological active contours on two ultrasound images (*medical1* and *medical2*) of breast nodules.

A. Operator composition

Let T_h^1 and T_h^2 be any two morphological operators, and let L_h^1 and L_h^2 be their corresponding infinitesimal operators. We can write a first order approximation to the operator composition $T_{h/2}^2 \circ T_{h/2}^1$ as

$$\begin{aligned} T_{h/2}^2 \circ T_{h/2}^1 u &\approx T_{h/2}\left(u + \frac{h}{2} L_h^1(u)\right) \\ &\approx u + \frac{h}{2} L_h^1(u) + \frac{h}{2} L_h^2\left(u + \frac{h}{2} L_h^1\right) \\ &\approx u + \frac{h}{2} L_h^1(u) + \frac{h}{2} L_h^2(u) + \\ &\quad + \left(\frac{h}{2}\right)^2 L_h^2 L_h^1(u). \end{aligned} \tag{20}$$

The last term depends on the squared value of h, and it can be dismissed for a small h,

$$\begin{aligned} T_{h/2}^2 \circ T_{h/2}^1 u &\approx \frac{u + hL_h^1(u)}{2} + \frac{u + hL_h^2(u)}{2} \\ &\approx \frac{1}{2}(T_h^2 u + T_h^1 u). \end{aligned} \tag{21}$$

Therefore, this approximation becomes accurate for small values of h, and we can replace $\frac{1}{2}(T_h^2 u + T_h^1 u)$ by the composition $T_{h/2}^2 \circ T_{h/2}^1 u$.

References

[1] D. Adalsteinsson and J. A. Sethian. A fast level set method for propagating interfaces. *Journal of Computational Physics*, 118(2):269–277, 1995.

[2] V. Caselles, R. Kimmel, and G. Sapiro. Geodesic active contours. *International Journal of Computer Vision*, 22(1):61–79, 1997.

[3] F. Catté, F. Dibos, and G. Koepfler. A morphological scheme for mean curvature motion and applications to anisotropic diffusion and motion of level sets. *SIAM Journal on Numerical Analysis*, 32(6):1895–1909, 1995.

[4] L. D. Cohen. On active contour models and balloons. *CVGIP: Image Understanding*, 53(2):211–218, 1991.

[5] R. Goldenberg, R. Kimmel, E. Rivlin, and M. Rudzsky. Fast geodesic active contours. *IEEE Transactions on Image Processing*, 10(10):1467–1475, 2001.

[6] F. Guichard, J. Morel, and R.Ryan. *Contrast invariant image analysis and PDE's*. `http://mw.cmla.ens-cachan.fr/~morel/JMMBookOct04.pdf`.

[7] R. Kimmel. *Numerical Geometry of Images: Theory, Algorithms, and Applications*. Springer Verlag, 2003.

[8] S. Osher and J. A. Sethian. Fronts propagating with curvature-dependent speed: algorithms based on hamilton-jacobi formulations. *J. Comput. Phys.*, 79(1):12–49, 1988.

[9] N. Paragios, O. Mellina-Gottardo, and V. Ramesh. Gradient vector flow fast geometric active contours. *IEEE Transactions on Pattern Analysis and Machine Intelligence*, 26(3):402–407, 2004.

[10] Y. Shi and W. C. Karl. Real-time tracking using level-sets. In *Proc. International Conference on Computer Vision and Pattern Recognition*, 2005.

[11] T. Yoo, M. Ackerman, W. Lorensen, W. Schroeder, V. Chalana, S. Aylward, D. Metaxas, and R. Whitaker. Engineering and algorithm design for an image processing API: A technical report on ITK - the insight toolkit. *Proc. of Medicine Meets Virtual Reality, J. Westwood, ed., IOS Press Amsterdam*, pages 586–592, 2002.